Available online at www.sciencedirect.com
SCIENCE DIRECT
Journal of Catalysis 229 (2005) 459–469
JOURNAL OF CATALYSIS
www.elsevier.com/locate/jcat

Studies on the redox properties of chromite perovskite catalysts for soot combustion

Nunzio Russo, Debora Fino *, Guido Saracco, Vito Specchia

Materials Science and Chemical Engineering Department, Politecnico di Torino, Corso Duca degli Abruzzi 24, 10129 Torino, Italy

Received 10 September 2004; revised 18 November 2004; accepted 22 November 2004

Available online 28 December 2004

Abstract

This paper deals with the preparation (by combustion synthesis), the characterization (by XRD, AAS, BET, SEM, TEM, TPD/R, and XPS analyses), the catalytic activity testing (in a temperature-programmed combustion microreactor and in a DSC analyzer), and the assessment of the reaction mechanism of a series of nanostructured soot combustion catalysts based on La–Cr substoichiometric or alkali-metal-substituted perovskites ($La_{0.9}CrO_3$, $La_{0.8}CrO_3$, $La_{0.9}Na_{0.1}CrO_3$, $La_{0.9}K_{0.1}CrO_3$, $La_{0.9}Rb_{0.1}CrO_3$, $La_{0.8}Cr_{0.9}Li_{0.1}O_3$), whose performance is compared with that of the standard $LaCrO_3$. Some conclusions are drawn concerning the role of each single constituting element on the activity of the most promising catalyst, $La_{0.8}Cr_{0.9}Li_{0.1}O_3$, which is already active well below 400 °C. The role of weakly chemisorbed O^- surface species in particular is pointed out as crucial for the soot combustion process. This indicates the way for the development of new, more active catalysts, possibly capable of delivering amounts of these oxygen species even higher than those obtained (about 700 μmol/g) for the most active Li-substituted lanthanum chromite catalyst developed.

Keywords: Perovskite-type alkali-substituted chromites; Catalytic combustion; Diesel particulate; Soot; Suprafacial oxygen

1. Introduction

An intensive research has been carried out in the last decade to find catalysts active for the abatement of diesel exhaust pollutants. The main contaminants emitted by this type of engine are nitrogen oxides and soot particles. However, while the formation of nitrogen oxides in internal combustion engines is well understood, the formation of soot is by far more complicated and difficult to examine. The fulfillment of stricter emission regulations without affecting the fuel economy of diesel engines represents a real challenge. Soot and nitrogen oxides behave here like antagonists. Limited soot production is generally obtained at the price of a large NO formation, and vice versa. The current tendency is to minimize NO_x production by high exhaust gas recirculation (EGR) rates and tackle the problem of high diesel particulate emissions with the combined use of traps and oxidation catalysts [1].

Diesel particulate filters (DPFs) based on wall-flow-type monoliths are generally recognized as the most viable solution to the related pollution problem [2]. The filter durability is closely related to the successful control of the periodic regeneration by combustion of the deposited particulate. A timely regeneration prevents undesired backpressure buildup related to the soot accumulated in the filter. Since the temperature of the exhaust gases of modern diesel engines is relatively low (150–400 °C), well below the ignition temperature of diesel particulate in air (550–600 °C), the oxidation reaction might be fruitfully supported by a catalyst deposited in the trap. However, any attempt to achieve a completely "passive" regeneration of the trap has been frustrated by insufficient catalyst activity or stability [3–12]. Hence, fuel post-injection via a proper control of the common rail system and its combustion in an oxidation catalyst placed ahead

* Corresponding author. Fax: +39 011 5644699.
E-mail address: debora.fino@polito.it (D. Fino).

0021-9517/$ – see front matter
doi:10.1016/j.jcat.2004.11.025

of the trap is the commonly adopted procedure for occasionally increasing the trap temperature. This helps ignite the catalytic combustion of the trapped soot, eventually leading to filter regeneration [13]. Any catalyst to be placed over the trap should possess high thermochemical stability and intrinsic activity, to reliably ignite the soot as early as possible, thereby limiting the amount of post-injected fuel (a net loss from the economic viewpoint). It should also possess a microstructure capable of maximizing the contact points with the trapped soot without increasing the pressure drop too much. Therefore, a rational catalyst design for this system has been addressed. From this perspective, a previous paper of ours [14] addressed the development of very active perovskite (ABO_3) catalysts for the combustion of soot and analysis of the role played by suprafacial and intrafacial oxygen species over the catalyst surface in the carbon combustion process.

In this work, starting from the basic $LaCrO_3$ perovskite, several quite active catalysts, outperforming previously developed ones [14], are achieved by induction of charge deficiency at the A or B site by introduction of alkali metal elements or simply by promotion of A-site substoichiometry. An analysis of the reaction mechanism, mainly based on the interpretation of TPD/R and XPS characterization results, is also provided, which shows the importance of suprafacial oxygen species for the soot oxidation activity.

2. Experimental

2.1. Catalyst preparation

The following perovskite catalysts were prepared: $LaCrO_3$, $La_{0.9}CrO_3$, $La_{0.8}CrO_3$, $La_{0.9}Na_{0.1}CrO_3$, $La_{0.9}K_{0.1}CrO_3$, $La_{0.9}Rb_{0.1}CrO_3$, and $La_{0.8}Cr_{0.9}Li_{0.1}O_3$. The rationale for this selection was the introduction of an equal molar amount of alkali metal (0.1 mole per perovskite mole) in the perovskite structure. Most alkali metals considered (Na, K, Rb) are hosted at the A site of the perovskite because of their comparatively large size, whereas the small Li ion naturally becomes located at the B site. As La substoichiometry was found to pay off in terms of catalytic activity, as discussed later, it was maximized in the perovskite sample containing Li. The two substoichiometric $La_{0.9}CrO_3$ and $La_{0.8}CrO_3$ catalysts, holding no alkali metals in their structure, were then synthesized to provide a suitable reference for the assessment of the effect of alkali metal presence in the perovskites.

The preparation method employed was the so-called combustion synthesis, based on a highly exothermic and self-sustaining reaction [15]. This technique is particularly suited for the production of nanosized particles of catalyst. A nanostructured catalyst coating over the trap could effectively improve the local catalyst–soot contact conditions, a critical issue in this field, as mentioned earlier.

The synthesis process can be formally split into two steps (the preparation of lanthanum chromite is here considered as an example):

$$2La(NO_3)_3 + 2Cr(NO_3)_3 \rightarrow 2LaCrO_3 + 6N_2 + 15O_2, \quad (1)$$

$$10CO(NH_2)_2 + 15O_2 \rightarrow 10CO_2 + 20H_2O + 10N_2. \quad (2)$$

This is a very simplified view of a much more complex process that is far from being completely understood. Some deeper details of the present level of understanding of the process are provided in [15]. Reaction (1) is endothermic and represents the perovskite synthesis starting from the metal nitrate precursors, and reaction (2) is exothermic and accounts for the reaction between the oxygen derived from nitrate decomposition and urea. Some direct urea decomposition and combustion with atmospheric oxygen cannot be excluded. The preparation is in fact carried out in air within an electric oven kept at 600 °C, in which is placed a porcelain vessel that holds the precursors mixture (see [15] for further details). Stoichiometric amounts of metal nitrates (Fluka) were employed in the preparations, whereas the amount of urea used was 3.5-fold higher than stoichiometry so as to compensate for the effect of the above-mentioned parasitic reactions.

The overall set of reactions is markedly exothermic, which leads to a thermal peak within the reacting solid mixture well exceeding 1000 °C for a few seconds. Some NH_4NO_3 was added to the precursors mixture (1 g NH_4NO_3/g perovskite) to emphasize this sudden heat release, as indicated in [15]. Under these conditions, nucleation of perovskite crystals is induced, their growth is limited, and nanosized grains can be obtained. About 2 g of each perovskite catalyst was produced per preparation run.

After preparation, all catalysts were ground in a ball mill at room temperature and submitted to physical and chemical characterization.

A specific aging treatment was performed on the best performing catalyst ($La_{0.8}Cr_{0.9}Li_{0.1}O_3$) to check preliminary its potential deactivation in the presence of some gaseous components present in real diesel exhaust gases. A sample of the catalyst was kept in an oven at 600 °C for 24 h under a gas flow of the following composition: $SO_2 = 500$ ppm; water vapor = 12%; $CO_2 = 20\%$; oxygen = 4%; nitrogen = balance.

2.2. Fresh/aged catalyst characterization

Catalyst characterization was accomplished through several techniques:

2.2.1. X-Ray studies

X-ray diffraction (PW1710 Philips diffractometer equipped with a monochromator for the Cu-K_α radiation) was used on all fresh catalysts to determine whether the desired perovskite structure was actually obtained.

2.2.2. BET surface area

The BET specific surface areas of the prepared catalysts were evaluated from the linear parts of the BET plot of the N_2 isotherms with a Micromeritics ASAP 2010 analyzer. For bulk and nonporous catalysts, such as the perovskite type, the specific surface area can be directly related to the average crystal size.

2.2.3. TEM studies

Direct observation of the nanosized perovskite crystals was performed by transmission electron microscopy (TEM) (Philips CM 30 T).

2.2.4. FESEM analysis

A field emission scanning electron microscope (FESEM) (Leo 50/50 VP with Gemini column) was used to analyze the microstructure of the crystal aggregates of the catalysts.

2.2.5. Atomic absorption analysis (AAS)

Compositional analysis (dissolution in HNO_3/HCl followed by atomic absorption analysis with a Perkin–Elmer 1100B spectrometer) was performed on all prepared samples to confirm that the expected elemental compositions were achieved.

2.2.6. XPS studies

X-ray photoelectron spectroscopy was used to characterize the surface composition of some perovskite-based catalysts: the basic $LaCrO_3$ perovskite, the most active catalysts developed (i.e., $La_{0.8}Cr_{0.9}Li_{0.1}O_3$), a representative of the A-site-substituted perovskites ($La_{0.9}Na_{0.1}CrO_3$), and the reference $La_{0.8}CrO_3$ substoichiometric perovskite. The XPS analyses were carried out with a VG Escalab 200-C X-ray photoelectron spectrometer and a nonmonochromatic Mg-K_α source. A pass energy of 20 eV, a resolution of 1.1 eV, and a step of 0.2 eV were used for high-resolution spectra. We eliminated the effects of sample charging by referring the spectral line shift to the C 1s binding energy value of 284.6 eV. The XPS measurements were performed on the catalysts after two different thermal treatments: 60 min at 600 °C in pure oxygen with a pressure value of 1.1 bar (oxidizing condition) and 2 h at 400 °C in ultrahigh vacuum ($< 2 \times 10^{-9}$ mbar; reducing condition).

This XPS apparatus could also provide a quantitative analysis of the catalyst surface composition. For this purpose, the areas below the XPS peaks were determined with the software ECLIPSE v3.1 VG Scientific and the peak-fitting techniques for the Cr $2p_{3/2}$, La $3d_{5/2}$, and O 1s regions; peak areas were then normalized, with the Shirley background [16] and the Scofield [17] sensibility factors taken into account.

2.3. Catalytic activity tests

The catalytic activity of the prepared catalysts was tested in a temperature-programmed combustion (TPC) apparatus. A detailed description of the TPC equipment has appeared in a previous paper of ours [14]. This equipment mainly consists of a fixed bed inserted in a quartz microreactor (i.d. 4 mm). We prepared the fixed bed by mixing 50 mg of a 1:9 mixture (by weight) of carbon and powdered catalyst with 150 mg of silica pellets (0.3–0.7 mm in size); this inert material was adopted to reduce the specific pressure drop across the reactor and to prevent thermal runaways. Amorphous carbon particles by Cabot Ltd. were used for the sample preparation (about 45 nm in diameter; BET specific surface area = 200 m^2/g; 0.34% ashes after calcination at 800 °C; 12.2% adsorbed water moisture; no adsorbed hydrocarbons and sulfates). This type of carbon was used because it burns at temperatures close to those characteristic of diesel particulate combustion. The catalyst–carbon mixture was obtained by careful grinding in an agate mortar. This corresponds to contact conditions that are generally referred to as "tight" [18], which are too intensive compared with what is actually achievable in a catalytic soot trap, but they permit a much higher degree of reproducibility, which sets a good basis for activity screening studies.

The catalyst/carbon/SiO_2 mixture was inserted in the reactor and confined between two quartz-wool layers. The reactor was placed in a PID-regulated oven, and a K-type thermocouple was inserted in the packed bed. We carried out the tests by heating the fixed bed to 700 °C (heating rate 5 °C/min) with a mass flow meter that fed an air flow to the microreactor (100 Nml/min). The carbon conversion was indirectly monitored with a NDIR analyzer (Elsag-Bailey for NO, CO, CO_2, SO_2) that measured the carbon monoxide and dioxide concentration in the outlet gases. The carbon mass balance was always verified within a 4% error. A computer recorded both the fixed-bed temperature and the CO and CO_2 outlet concentrations as a function of time. The CO_2 outlet concentration at the beginning of the run increases, starting from the carbon ignition temperature, reaches a maximum, and then decreases as a consequence of carbon consumption. The temperature corresponding to the CO_2 peak (T_p) was taken as an index of the activity of each tested catalyst: the lower the T_p value, the more active the catalyst. The runs were repeated three times, and the average T_p value was assumed for each catalyst. The maximum deviation between the three T_p values never exceeded 20 °C. To fully examine the catalytic effect of the perovskites, blank soot combustion runs in the absence of any catalyst and in the presence of only inert SiO_2 were also carried out.

2.4. Activation energy assessment by the Ozawa method

The activation energy of soot combustion over the prepared catalysts was measured according the Ozawa method (described below) on the basis of DSC runs carried out in a Perkin–Elmer DSC-Pyris equipment. Ten milligrams of a 9:1 (by weight) catalyst/carbon mixture was analyzed (with the same weight of alumina as a reference) during a temperature scan from 50 to 720 °C (heating rates: $\phi = 5$, 10, 20,

30, and 50 °C/min). An air flow (10 ml/min) provided the oxygen required for carbon combustion. Thus DSC patterns were processed to obtain the onset and maximum temperatures of the exothermic combustion peak. DSC scans were also performed (under the experimental conditions reported above) on an alumina/carbon mixture, so as to estimate the activation energy of the noncatalyzed carbon combustion.

The activation energy can be evaluated through the so-called Ozawa procedure [19,20] by a proper interpretation of thermal analysis data. According to this method, the following relationship links the values of the heating rate with the corresponding values of temperature (T_α) at which a fixed fraction α of carbon is burned during each run:

$$\ln\phi = B - 0.4567\left(\frac{E_a}{RT_\alpha}\right), \tag{3}$$

where B is a constant lumping α-dependent terms. If the heat released by the combustion is assumed to be proportional to the fraction α of converted carbon, once a reference α value is chosen (e.g., 25, 50, 75%), the T_α value corresponding to such an α value can easily be derived from the DSC curves by evaluation, via a simple integration, of the amount of heat released by the combustion. Estimates of the activation energy can be calculated from the slope of the best-fitting line by least-square fitting of the $\ln\phi$-vs-$1/T_\alpha$ data series.

2.5. TPD-TPR analysis

Some further analyses were performed on all of the prepared perovskites in a Thermoquest TPD/R/O 1100 analyzer, equipped with a thermal conductibility (TCD) detector and a quadrupole (MS) detector (Baltzer Quadstar 422). A fixed bed of catalyst was enclosed in a quartz tube and sandwiched between two quartz wool layers; before each temperature-programmed desorption (TPD) run, the catalyst was heated under an O_2 flow (40 Nml/min) up to 750 °C. After 30 min at this temperature as a common pretreatment, the reactor temperature was then lowered to room temperature with the same flow rate of oxygen, thereby allowing complete oxygen adsorption over the catalyst. Afterward, helium was fed to the reactor at a rate of 10 ml/min, which was kept up for 1 h at room temperature to purge any excess oxygen molecules. The catalyst was then heated to 1100 °C at a constant rate of 10 °C/min under a helium flow rate of 10 Nml/min. The total amount of O_2 desorbed during the heating protocol was analysed by the TCD detector after proper calibration.

Temperature-programmed reduction (TPR) experiments were carried out in the same apparatus. After the same oxidation pretreatment as adopted for the TPD runs, the sample was reduced with a 4.95% H_2/Ar mixture (10 Nml/min) as it was heated at a rate of 10 °C/min to 1100 °C. Once again the amount of H_2 converted could be monitored via the TCD detector.

X-ray diffraction was once again used on the catalysts, which underwent TPD or TPR analysis, to check whether the perovskite structure had been retained or not, and to check for the possible appearance of new phases.

3. Results and discussion

Fig. 1 illustrates the diffraction spectra recorded for all of the catalysts synthesized in the present study: it confirms the presence of a crystalline lanthanum chromite phase (JPCDS card: PDF 83-1328). However, since the detection limit of

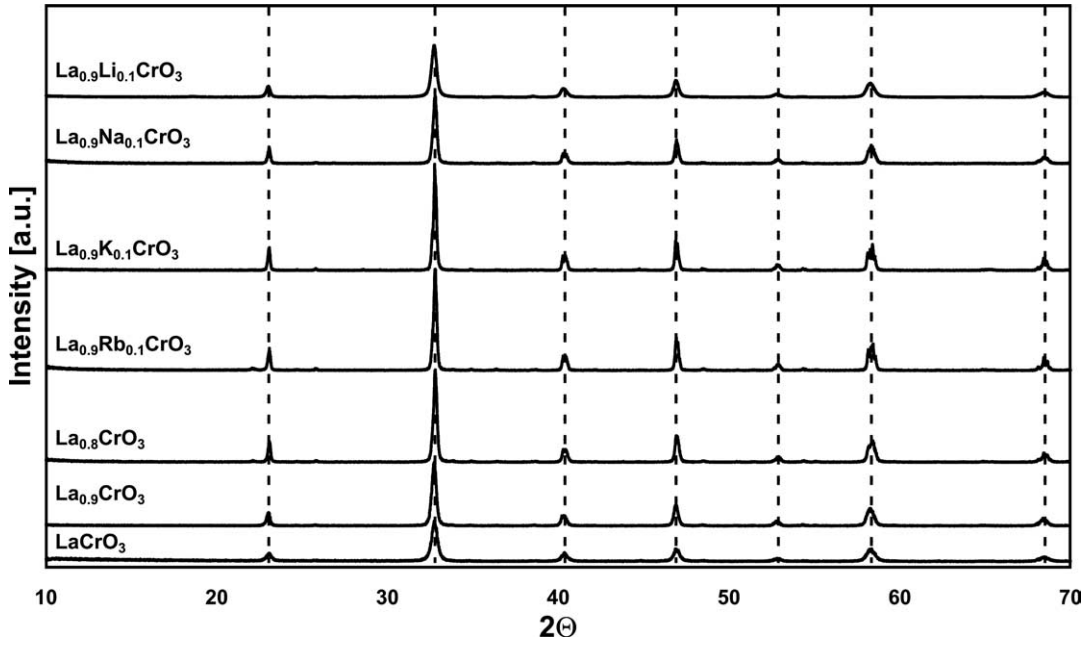

Fig. 1. XRD diffraction patterns of all the catalysts synthesized; vertical dot lines are located according to PDF 83-1328 $La_{0.985}CrO_{2.9775}$ card.

this technique is 4 wt%, the presence of amorphous or minor crystalline phases cannot be excluded. Atomic absorption analysis (AAS) confirmed that the overall amount of the various elements of interest (La, Rb, K, Na, Cr, Li) was consistent with that used in the precursors and was compatible with the phases detected by X-ray diffraction. The results of atomic adsorption analysis are listed in Table 1.

Fig. 2a shows a TEM picture of $La_{0.8}Cr_{0.9}Li_{0.1}O_3$ perovskite catalyst produced via combustion synthesis. It refers to the catalyst that showed the highest activity among those prepared. However, it is representative of all of the crystal sizes of the prepared catalysts, except for $La_{0.9}Rb_{0.1}CrO_3$,

Table 1
Chemical composition of the prepared perovskite catalysts as detected by AAS (molar ratios referred to La)

Catalyst	La	Cr	Li	Na	Rb	K
$LaCrO_3$	1	1.008	–	–	–	–
$La_{0.9}CrO_3$	1	1.115	–	–	–	–
$La_{0.8}CrO_3$	1	1.257	–	–	–	–
$La_{0.8}Cr_{0.9}Li_{0.1}O_3$	1	1.127	0.126	–	–	–
$La_{0.9}Na_{0.1}CrO_3$	1	1.113	–	0.112	–	–
$La_{0.9}Rb_{0.1}CrO_3$	1	1.114	–	–	0.113	–
$La_{0.9}K_{0.1}CrO_3$	1	1.113	–	–	–	0.112

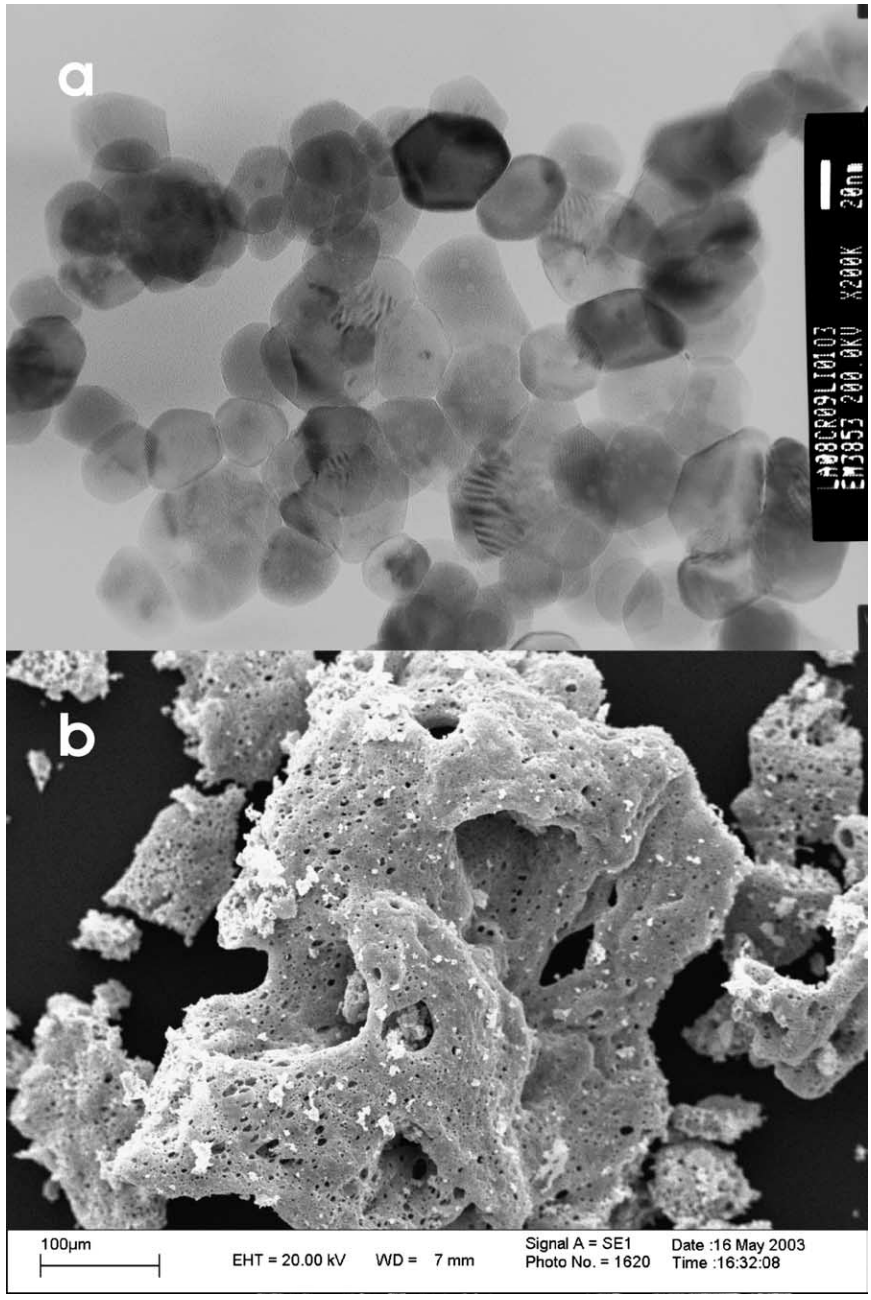

Fig. 2. Electron microscopy results concerning the $La_{0.8}Cr_{0.9}Li_{0.1}O_3$ catalyst: (a) TEM micrograph of the catalyst crystals; (b) FESEM view of the catalyst microstructure.

Table 2
Collection of results of catalyst characterization tests concerning catalytic activity, activation energy, BET specific surface area and temperature programmed desorption of oxygen

Catalyst	T_p (°C)	E_a (kJ/mol)	BET (m^2/g)	Desorbed (μmol/g)	
				α O_2	β O_2
$LaCrO_3$	495	147.0	17.53	8.0	15.3
$La_{0.9}CrO_3$	447	133.8	16.46	188.0	145.5
$La_{0.8}CrO_3$	441	130.2	13.54	103.1	74.0
$La_{0.8}Cr_{0.9}Li_{0.1}O_3$	408	125.5	12.96	529.0	209.7
$La_{0.9}Na_{0.1}CrO_3$	455	134.5	17.09	50.9	364.1
$La_{0.9}Rb_{0.1}CrO_3$	448	148.9	7.72	18.4	215.2
$La_{0.9}K_{0.1}CrO_3$	454	127.7	17.62	34.7	211.4
Non-catalytic combustion	650	159.0	–	–	–

whose crystals are slightly larger than those of the other perovskites. Most of the perovskite crystals range between 20 and 50 nm in size, which is perfectly in line with the BET specific surface areas measured (about 15 m^2/g on average; see Table 2). In fact it is easy to calculate that the above range size should correspond approximately to specific surface areas in the range of 8–23 m^2/g, once we assume the average density of the catalyst particles is 6500 kg/m^3 [21], and we assume an average value for the perovskites tested and a spherical shape for the particles themselves. Finally, no indications of the possible presence of amorphous or minor crystalline phases is perceivable in Fig. 2a or in any TEM observation made on $La_{0.8}Cr_{0.9}Li_{0.1}O_3$ or any other catalyst.

The microstructure of the catalyst crystals agglomerates looks rather spongy (Fig. 2b). This is a consequence of the sudden release of a large amount of gases during the combustion synthesis, owing to the decomposition/combustion of the reacting precursors. Such a microstructure fosters the formation of highly corrugated interfaces of the catalyst powder agglomerates, which in turn intensifies the contact between the catalyst and the soot. In the present context, perovskite crystals with a size on the same order of magnitude as that of the particulate (100 nm on average for the last generation of Common Rail Engines [22]) are expected to provide the highest specific number of contact points between these two counterparts.

Shifting to the activity screening results, Fig. 3 shows the TPC plots obtained with each catalyst tested, the peak temperatures of which are listed in Table 2 together with the T_p value of noncatalytic combustion (650 °C). As expected, all of the catalysts significantly lower the combustion peak temperature compared with that of the noncatalytic combustion. An activity order can be outlined as

1) the $La_{0.8}Cr_{0.9}Li_{0.1}O_3$ shows the best activity by far ($T_p = 408$ °C);
2) the aging treatment in the presence of SO_2, H_2O, and CO_2 leads to a limited deactivation of this catalyst ($T_p = 422$ °C);
3) the other perovskite catalysts characterized by lanthanum deficiency (i.e., $La_{0.8}CrO_3$, $La_{0.9}CrO_3$, $La_{0.9}Na_{0.1}CrO_3$, $La_{0.9}Rb_{0.1}CrO_3$, $La_{0.9}K_{0.1}CrO_3$) exhibit quite similar activities (T_p ranging from 441 to 455 °C);
4) the unsubstituted $LaCrO_3$ chromite is by far the least active catalyst ($T_p = 495$ °C).
5) the CO_2 selectivity of the best performing catalyst ($La_{0.8}Cr_{0.9}Li_{0.1}O_3$) as prepared was 96%, the other catalysts being characterized by lower values but never less than 87% ($LaCrO_3$).

In line with an earlier paper of ours [23], it can be deduced that replacement of some of the lanthanum with a lower valence alkali metal brings about the formation of high-valence chromium (Cr^{HV}) to maintain electroneutrality and possibly to obtain more active or more concentrated oxygen species over the catalyst surface.

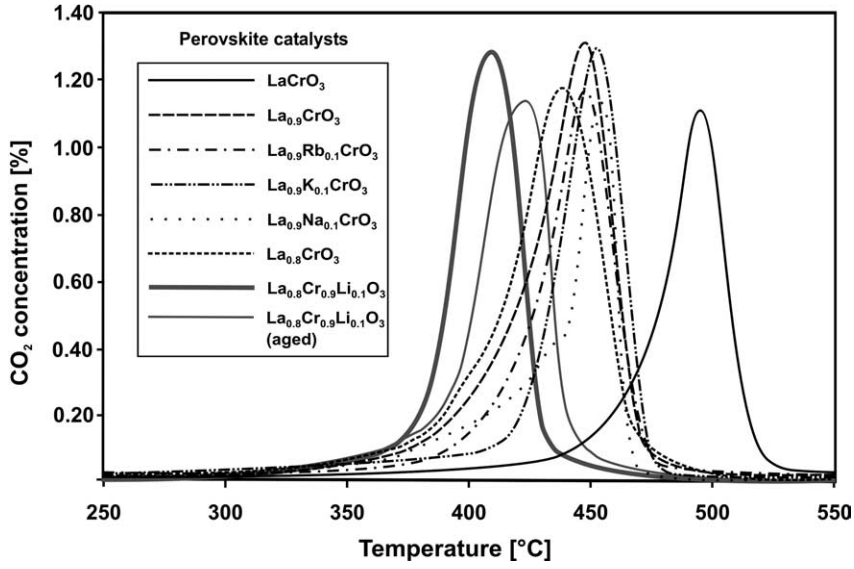

Fig. 3. Results of the TPC runs performed with all the selected perovskite catalysts.

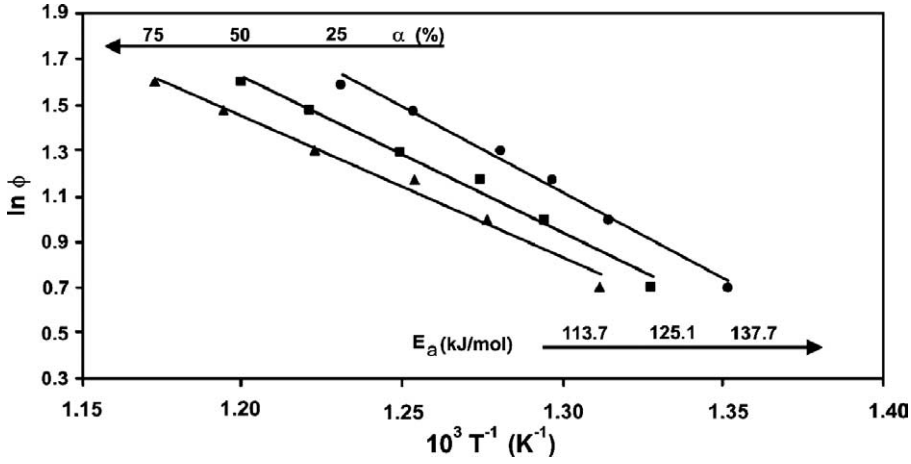

Fig. 4. Ozawa plots for the determination of the activation energy of soot combustion over the $La_{0.8}Cr_{0.9}Li_{0.1}O_3$ catalyst.

The activation energies of carbon combustion over all of the catalysts can be analyzed to better elucidate this point. In this context, Fig. 4 shows, as an example, a typical Ozawa plot related to the most active catalyst ($La_{0.8}Cr_{0.9}Li_{0.1}O_3$), whereas Table 2 lists the activation energy values calculated for all of the catalysts studied. It has to be admitted that, on the grounds of the basic assumptions of the Ozawa method, and taking into account the high exothermic nature of the reaction studied and the fast heating rates adopted, the activation energies measured by this method might contain an error of about ±5%. Under these circumstances, one may nonetheless conclude that all the catalysts lower the activation energy compared with the noncatalytic combustion. However, their activation energy values are not very different from one another, which seems to entail the possibility that the different perovskites are capable of delivering oxygen species of a similar nature or reactivity to the carbon particulates. As a consequence, the main reason for the superior activity of chromites should lie in a significantly different surface concentration of active oxygen species. It should be pointed out, however, that the most active catalyst ($La_{0.8}Cr_{0.9}Li_{0.1}O_3$) also shows the lowest activation energy value (125.5 kJ/mol).

Transient thermal analysis studies (TPD/TPR) were quite helpful in elucidating this issue. In particular, Fig. 5a shows the results obtained during oxygen TPD runs. As thoroughly discussed in a review by Seyama [24] and in a number of papers (e.g., [25–27]), perovskites can desorb two different types of oxygen species at high temperatures: a low-temperature species, named α, desorbed in the 300–600 °C range, and a high-temperature one, named β, desorbed above about 600 °C. The α desorption peak is not always perceivable in TPD plots and strongly depends on the concentration of surface oxygen vacancies. In particular, its onset and intensity depend primarily on the degree of substitution of the A ion with ions of lower valence, but also on the nature of the B metal of the ABO_3 structure [25]. Conversely, the β peak is strictly related to the nature of the B ion, and its occurrence is strictly linked to redox transitions of the valence state of this ion, which is chromium in the present case.

The TPD curves in Fig. 5a thus seem to suggest that α- and not β-type oxygen should be responsible for the superior activity of chromites toward soot combustion. Table 2 lists the amount of α and β oxygen species evaluated by integration of the TPD curves.

If attention is focused on the temperature range below 500 °C, well inside the α oxygen region, where the most active perovskites tested displayed their best soot combustion activities (see the CO_2 peaks in Fig. 3), Fig. 5a shows that the three most active perovskites ($La_{0.8}Cr_{0.9}Li_{0.1}O_3$, $La_{0.8}CrO_3$, $La_{0.9}CrO_3$) display significant oxygen desorption in this temperature range (see the superior amount of α oxygen desorbed by the $La_{0.9}CrO_3$ and $La_{0.8}Cr_{0.9}Li_{0.1}O_3$ in Table 2), or, at least, as for the $La_{0.8}CrO_3$ sample, they display significant oxygen desorption at very low temperatures. Both the amount and the temperature at which α oxygen is released seem thus to be the governing parameters for the catalytic activity. In line with earlier studies [14], such α-type, weakly chemisorbed "suprafacial" species are likely those responsible for soot combustion. It is perhaps possible that these α-type oxygen species could undergo *spillover* [1,28] over the carbon agglomerates in contact with the catalyst. This would result in an increase in the number of sites in which oxygen reacts with the carbon particles per unit time, which entails a significant increase in reaction kinetics.

By comparing the temperatures at which the TPC and TPD curves of the most active catalyst ($La_{0.8}Cr_{0.9}Li_{0.1}O_3$) take place, it might be questioned whether the α-oxygen spontaneously desorbed by the catalyst at temperatures higher than 450 °C might actually be responsible for carbon oxidation in the temperature range 300–450 °C, at which most of the CO_2 production occurs during the TPC run. A specific TPD analysis, performed under pure He flow on a 9:1 catalyst-to-carbon mixture equal to that used in TPC experiments, clarified that, even in the absence of oxygen in the gas phase, the soot is capable of reacting away the

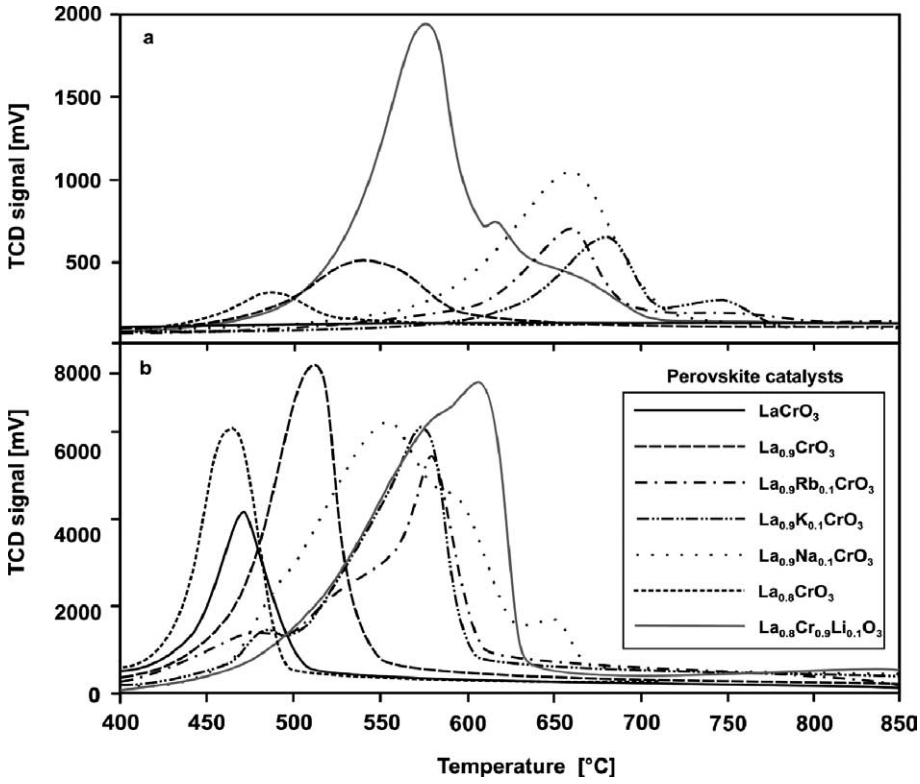

Fig. 5. Results of the temperature-programmed desorption (a) and reduction (b) tests on all the selected perovskite catalysts.

surface oxygen species to form CO_2 to a detectable extent, already slightly above 200 °C.

Conversely, in line with the literature data [29], it has to be stressed that chromite catalysts, beyond the suprafacial oxygen (α), do lose intrafacial oxygen (β) at high temperatures. A non-negligible fraction of oxygen is indeed released by most catalysts at temperatures higher than 600 °C. Only in the case of the basic $LaCrO_3$ does the total amount of released β oxygen seem to be quite limited (Table 2).

This type of oxygen should indeed dominate the behavior of the various perovskites during TPR runs (Fig. 5b). In general, the presence of hydrogen seems to anticipate the loss of oxygen compared with the TPD experiments. This anticipation leads to a very sharp and intensive reduction peak, likely lumping both α- and β-species. As opposed to carbon, which can only come in contact with suprafacial oxygen, hydrogen can indeed easily react away also the intrafacial oxygen type, without destroying the perovskite structure in the temperature range of interest. This was actually checked by XRD analysis.

As for the alkali-metal-substituted catalysts, it might be guessed that the presence of the electropositive alkali ions in the perovskite structure stabilizes the Cr^{HV} species and renders its bonding to β-type oxygen stronger than that for the basic chromite. The higher this strengthening effect, the more evident the shift toward high temperatures of the TPR peak, as compared with that of $LaCrO_3$. This feature does not seem to have any role in the combustion of soot, in which α-type oxygen should play a prevalent role. A sort of trade-off seems to hold for most alkali-metal-substituted catalysts tested: the higher the amount of α oxygen, indicated by an early and intensive TPD peak, the stronger the binding of β oxygen, indicated by a late TPR peak. Conversely, a different behavior was shown by substoichiometric samples carrying no alkali metals (i.e., $La_{0.8}CrO_3$ and $La_{0.9}CrO_3$), which release oxygen in both TPD and TPR runs at rather low temperatures.

To evaluate the valence state of the mentioned oxygen ions, as well as those of the transition metal Cr, core-level XPS spectra were measured for four samples (listed here in order of increasing catalytic activity): $LaCrO_3$, $La_{0.9}Na_{0.1}CrO_3$, $La_{0.8}CrO_3$, and $La_{0.8}Cr_{0.9}Li_{0.1}O_3$. As mentioned earlier, the samples were characterized after calcination in pure oxygen at 600 °C for 1 h (label: "600 °C O_2") and just after the second heat treatment at 400 °C in ultra-high vacuum (label: "400 °C UHV"). These two treatments were performed to simulate, within the XPS apparatus, the catalyst behavior before and after the oxidation activity toward diesel soot.

Let us first compare the results of the samples displaying the lowest ($LaCrO_3$) and the highest ($La_{0.8}Cr_{0.9}Li_{0.1}O_3$) catalytic activity. The photoelectron peaks of Cr $2p_{3/2}$ for the two catalysts after both the oxidation and reduction thermal treatments are depicted in Fig. 6. By performing a peak fitting deconvolution, we separated the chromium spectrum into two peaks: the "low valence" Cr^{LV} occurring at about 576 eV and the "high valence" Cr^{HV}, characterized by an average binding energy of about 579 eV. The first peak is

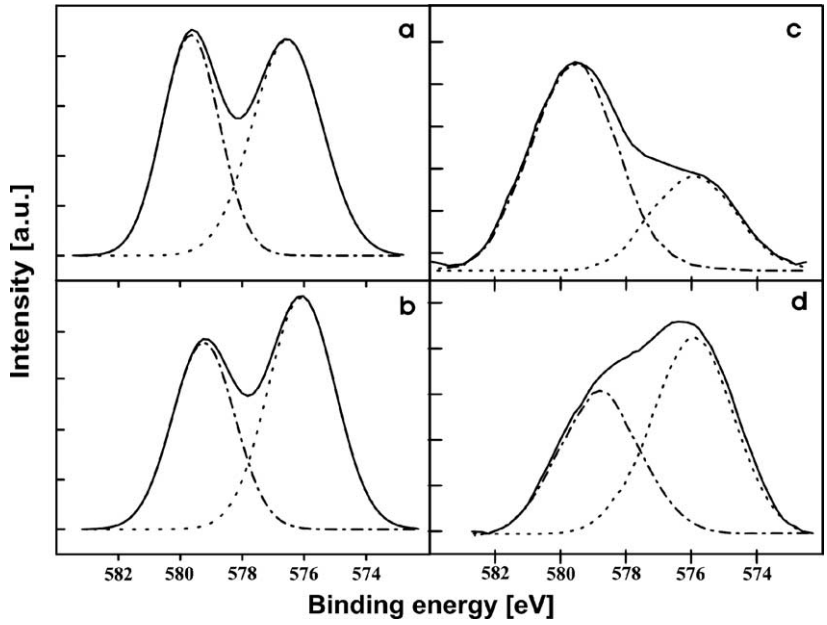

Fig. 6. X-ray photoelectron spectra in the Cr $2p_{3/2}$ region of: (a) $LaCrO_3$, 600 °C, O_2; (b) $LaCrO_3$, 400 °C, UHV; (c) $La_{0.8}Cr_{0.9}Li_{0.1}O_3$, 600 °C, O_2; (d) $La_{0.8}Cr_{0.9}Li_{0.1}O_3$, 400 °C, UHV. Dotted line: low valence Cr, dashed–dotted line: high valence Cr.

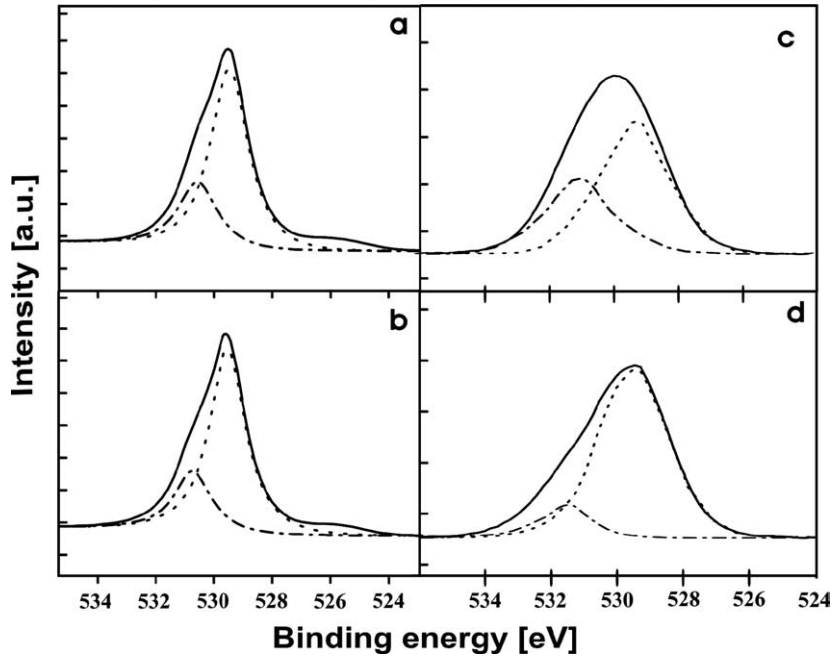

Fig. 7. X-ray photoelectron spectra in the O 1s region of: (a) $LaCrO_3$, 600 °C, O_2; (b) $LaCrO_3$, 400 °C, UHV; (c) $La_{0.8}Cr_{0.9}Li_{0.1}O_3$, 600 °C, O_2; (d) $La_{0.8}Cr_{0.9}Li_{0.1}O_3$, 400 °C, UHV. Dotted line: O^{2-} species; dashed–dotted line: O^-.

unequivocally assigned to Cr^{3+} [29–31]. The second peak, defined as "high valence," should be assigned to a higher valence chromium state, perhaps Cr^{5+} or Cr^{6+}. XPS data for the latter species are reported to lie in the range of 578.0–578.8 eV for Cr^{5+} in $LaCrO_4$ [32–34] and 579–580 eV for compounds containing Cr^{6+} [35,36].

Conversely, Fig. 7 shows the O 1s spectra of the same catalysts. Also in this case the signal deconvolution gave a double peak consistent with the reported data regarding substituted and unsubstituted ABO_3-type perovskite [36–40]. The peak with lower binding energy was generally assigned to a normal O 1s (O^{2-}) signal that corresponds to the lattice β-oxygen type. The peak at about 531 eV could instead be attributed to adsorbed oxygen, in the form of O^-, weakly bound to the catalyst surface (α-oxygen).

Incidentally, at about 526 eV the Auger peak of lanthanum was observed only for the $LaCrO_3$ sample because of the higher La surface atomic concentration with respect to

Table 3
Atomic percent concentrations of La, Cr and O species as derived from XPS analysis (600 °C O_2 = sample pre-treated at 600 °C under O_2 atmosphere; 400 °C UHV = sample pre-treated at 400 °C under high-vacuum conditions)

Catalyst samples	Atomic concentrations (%)								
	La	O	O^{2-}	O^-	O^-/O	Cr	Cr^{HV}	Cr^{LV}	Cr^{HV}/Cr
$La_{0.8}Cr_{0.9}Li_{0.1}O_3$, 600 °C O_2	19.0	62.1	38.5	23.6	0.61	18.9	10.4	8.5	1.22
$La_{0.8}Cr_{0.9}Li_{0.1}O_3$, 400 °C UHV	18.7	62.3	51.3	11.0	0.21	19.0	5.4	13.6	0.40
$La_{0.8}CrO_3$, 600 °C O_2	23.2	60.0	32.5	27.5	0.46	16.7	5.8	11.0	0.35
$La_{0.8}CrO_3$, 400 °C UHV	23.9	59.6	49.4	10.2	0.17	16.5	3.5	13.0	0.21
$La_{0.9}Na_{0.1}CrO_3$, 600 °C O_2	17.0	58.8	29.4	27.5	0.47	14.6	7.7	6.9	0.53
$La_{0.9}Na_{0.1}CrO_3$, 400 °C UHV	18.2	57.2	28.5	26.0	0.45	14.9	7.0	7.9	0.47
$LaCrO_3$, 600 °C O_2	25.3	60.7	45.1	15.6	0.25	14.0	4.8	9.2	0.30
$LaCrO_3$, 400 °C UHV	25.8	60.2	45.6	14.6	0.23	14.0	4.4	9.6	0.29

$La_{0.8}Cr_{0.9}Li_{0.1}O_3$. The XPS peak of lithium at about 55 eV was also observed for the substituted perovskite after the different thermal treatments. Unfortunately, quantitative analysis of Li was not possible due to the overlap of the above characteristic peak with the satellite peak of La 4d from Mg-K_β.

As anticipated, the atomic concentrations at the surface of the catalysts could be determined; these are listed in Table 3 for all of the catalysts analyzed by XPS, according to decreasing catalytic activity order.

The data in Table 3 generally reveal an excess of lanthanum, with respect to the stoichiometry, on the surface of the $LaCrO_3$ and $La_{0.8}CrO_3$ catalysts and surface concentration values equivalent to bulk values for the alkali-metal-substituted perovskites ($La_{0.9}Na_{0.1}CrO_3$ and $La_{0.8}Cr_{0.9}Li_{0.1}O_3$). Conversely, the chromium surface concentration was found to be significantly less than stoichiometric for the $LaCrO_3$, $La_{0.8}CrO_3$, and $La_{0.9}Na_{0.1}CrO_3$ compounds, whereas the oxygen content was found in slight excess only for the $La_{0.8}Cr_{0.9}Li_{0.1}O_3$ perovskite, which is perfectly in line with the large amount of oxygen desorbed by this material during TPD.

The partial atomic concentrations of both chromium and oxygen with different valences are also reported as evaluated from the plot in Figs. 6 and 7 or from equivalent plots for the $La_{0.8}CrO_3$ and $La_{0.9}Na_{0.1}CrO_3$ catalysts. The $LaCrO_3$ and $La_{0.8}Cr_{0.9}Li_{0.1}O_3$ catalysts (Figs. 6 and 7) showed quite different behavior when submitted to the two different thermal treatments. The surface composition of the unsubsituted perovskite remained practically unchanged. In contrast, the $La_{0.8}Cr_{0.9}Li_{0.1}O_3$ sample showed a deep difference between the reduced and the oxidized state, according to the analysis of the ratios Cr^{HV}/Cr and O^-/O, which decreased dramatically after exposure to high-vacuum conditions. The higher catalytic activity toward carbon combustion of the lithium-substituted chromite could thus be correlated with the capacity to enrich the surface with the more reactive O^- species, corresponding to the earlier mentioned α-oxygen type.

To further strengthen this hypothesis, it can easily be noticed that as long as the catalytic activity decreases (from the top to the bottom of Table 3), the variation in the Cr^{HV}/Cr parameter from the oxidized to the reduced state of the catalyst becomes less and less significant. This is a sign of the prevalent role of the redox cycles of Cr in the catalytic activity itself.

4. Conclusions

Several chromite catalysts ($LaCrO_3$, $La_{0.9}CrO_3$, $La_{0.8}CrO_3$, $La_{0.9}Rb_{0.1}CrO_3$, $La_{0.9}K_{0.1}CrO_3$, $La_{0.9}Na_{0.1}CrO_3$, $La_{0.8}Cr_{0.9}Li_{0.1}O_3$) were prepared by combustion synthesis, characterized, and tested as catalysts for soot combustion.

The Li-substituted chromite catalyst ($La_{0.8}Cr_{0.9}Li_{0.1}O_3$) exhibits the highest activity as a consequence of its greater amount of weakly chemisorbed O^- species (α-oxygen), which were pointed out as the key player in the soot oxidation state. This catalyst is currently being tested on real flue gases in innovative catalytic wall-flow traps.

In a parallel effort, catalytic materials characterized by the highest possible α-oxygen type concentration are currently being developed, with attention to their compatibility with either trap material or the poisoning components present in diesel exhaust gas (e.g., sulfur oxides).

Symbols

B	constant in the Ozawa method,
E_a	activation energy (kJ/mol),
R	ideal gas constant (= 8.314 J/(mol K)),
T	absolute temperature (K),
T_α	temperature at which a given α value is reached (K),
T_p	peak temperature of CO_2 production during soot combustion K.

Greek letters

α	fraction of converted soot,
ϕ	heating rate (K/s),
Θ	diffraction angle.

References

[1] B.A.A.L. van Setten, M. Makkee, J.A. Moulijn, Catal. Rev.-Sci. Eng. 43 (2001) 489.
[2] R.M. Herck, S. Gulati, R.J. Farrauto, Chem. Eng. J. 82 (2001) 149.
[3] C. Badini, G. Saracco, V. Serra, Appl. Catal. B 11 (1997) 307.
[4] C. Badini, G. Saracco, V. Serra, Appl. Catal. B 11 (1997) 329.
[5] G. Saracco, C. Badini, N. Russo, V. Specchia, Appl. Catal. B 21 (1999) 233.
[6] D. Fino, G. Saracco, V. Specchia, Industrial Ceramics 22 (2002) 37.
[7] P. Ciambelli, S. Cimino, S. De Rossi, M. Faticanti, L. Lisi, G. Minelli, I. Petitti, P. Porta, G. Russo, M. Turco, Appl. Catal. B 24 (2000) 243.
[8] P. Ciambelli, P. Corbo, M. Gambino, V. Palma, S. Vaccaro, Catal. Today 27 (1996) 99.
[9] P. Ciambelli, V. Palma, S. Vaccaro, Catal. Today 17 (1993) 71.
[10] G. Mul, J.P.A. Neeft, F. Kapteijn, M. Makkee, J.A. Moulijn, Appl. Catal. B 6 (1995) 339.
[11] J.P.A. Neeft, M. Makkee, J.A. Moulijn, Appl. Catal. B 8 (1996) 57.
[12] T.A. Nijhuis, S. Musch, M. Makkee, J.A. Moulijn, Appl. Catal. A 196 (2000) 217.
[13] D. Fino, P. Fino, G. Saracco, V. Specchia, Chem. Eng. Sci. 58 (2003) 951.
[14] D. Fino, N. Russo, G. Saracco, V. Specchia, J. Catal. 217 (2003) 367.
[15] A. Civera, M. Pavese, G. Saracco, V. Specchia, Catal. Today 83 (2003) 199.
[16] D.A. Shirley, Phys. Rev. B 5 (1972) 4709.
[17] J.H. Scofield, J. Electron Spectrosc. Relat. Phenom. 8 (1976) 129.
[18] B.A.A.L. van Setten, J.M. Schouten, M. Makkee, J.A. Moulijn, Appl. Catal. B 28 (2000) 253.
[19] T. Ozawa, J. Thermal Anal. 2 (1970) 301.
[20] T. Ozawa, J. Thermal Anal. 7 (1975) 601.
[21] R.H. Perry, D.W. Green, J.O. Maloney, Perry's Chemical Engineers' Handbook, sixth ed., McGraw-Hill Book Co., New York, 1984.
[22] M. Kostoglou, P. Housiada, A.G. Konstandopoulos, Chem. Eng. Sci. 58 (2003) 3273.
[23] G. Saracco, G. Scibilia, A. Iannibello, G. Baldi, Appl. Catal. B 8 (1996) 229.
[24] T. Seyama, Catal. Rev.-Sci. Eng. 34 (1992) 281.
[25] N. Yamazoe, Y. Teraoka, Catal. Today 8 (1990) 175.
[26] G. Saracco, F. Geobaldo, G. Baldi, Appl. Catal. B 20 (1999) 277.
[27] L. Forni, I. Rossetti, Appl. Catal. B 38 (2002) 29.
[28] D. Fino, N. Russo, C. Badini, G. Saracco, V. Specchia, AIChE J. 49 (2003) 2173.
[29] S. Ponce, M.A. Pena, J.L.G. Fierro, Appl. Catal. B 24 (2000) 193.
[30] W.Y. Howng, R.J. Thorn, J. Chem. Phys. Solids 41 (1980) 75.
[31] D.J. Lam, B.W. Veal, D.E. Ellis, Phys. Rev. B 22 (1980) 5730.
[32] H. Konno, H. Tachikawa, A. Furusaki, R. Furuichi, Anal. Sci. 8 (1992) 641.
[33] A. Trunschke, D.L. Hoang, J. Radnik, H. Lieske, J. Catal. 191 (2000) 456.
[34] G.C. Allen, P.M. Tucker, Inorg. Chim. Acta 16 (1976) 41.
[35] D. Shuttleworth, J. Phys. Chem. 84 (1980) 1629.
[36] K. Tabata, I. Matsumoto, S. Kohiki, J. Mater. Sci. 22 (1987) 1882.
[37] N. Gunasekaran, S. Rajadurai, J.J. Carberry, N. Bakshi, C.B. Alcock, Solid State Ionics 73 (1994) 289.
[38] G.R. Rao, D.D. Sarma, Mod. Phys. Lett. B 4 (1990) 277.
[39] J.L.G. Fierro, L.G. Tejuca, Appl. Surf. Sci. 27 (1987) 453.
[40] N. Yamazoe, Y. Teraoka, T. Seyama, Chem. Lett. (1981) 1767.